Original Article

MOLECULAR METABOLISM

Impact of metabolic stress induced by diets, aging and fasting on tissue oxygen consumption

Olena Mackert [1], Eva Katrin Wirth [1,2], Rongwan Sun [1,2], Jennifer Winkler [1], Aoxue Liu [1,2], Kostja Renko [3], Séverine Kunz [4], Joachim Spranger [1,2,*], Sebastian Brachs [1,2]

ABSTRACT

Objective: Alterations in mitochondrial function play an important role in the development of various diseases, such as obesity, insulin resistance, steatohepatitis, atherosclerosis and cancer. However, accurate assessment of mitochondrial respiration *ex vivo* is limited and remains highly challenging. Using our novel method, we measured mitochondrial oxygen consumption (OCR) and extracellular acidification rate (ECAR) of metabolically relevant tissues *ex vivo* to investigate the impact of different metabolic stressors on mitochondrial function.

Methods: Comparative analyses of OCR and ECAR were performed in tissue biopsies of young mice fed 12 weeks standard-control (STD), high-fat (HFD), high-sucrose (HSD), or western diet (WD), matured mice with HFD, and 2year-old mice aged on STD with and without fasting.

Results: While diets had only marginal effects on mitochondrial respiration, respiratory chain complexes II and IV were reduced in adipose tissue (AT). Moreover, matured HFD-fed mice showed a decreased hepatic metabolic flexibility and prolonged aging increased OCR in brown AT. Interestingly, fasting boosted pancreatic and hepatic OCR while decreasing weight of those organs. Furthermore, ECAR measurements in AT could indicate its lipolytic capacity.

Conclusion: Using *ex vivo* tissue measurements, we could extensively analyze mitochondrial function of liver, AT, pancreas and heart revealing effects of metabolic stress, especially aging.

Keywords Mitochondrial respiration; Metabolic stress; Diet; Age; Fasting; Oxygen consumption rate

1. INTRODUCTION

Mitochondria convert the energy stored in nutrients into ATP and other utilizable forms. Moreover, they are involved in the production and elimination of reactive oxygen species (ROS). Therefore, mitochondria have the capacity to adapt to altered physiological conditions, such as increased energy requirements or changed environmental factors and are thus crucial for cellular homeostasis [1]. However, pathological conditions, for instance long-term excessive supply of nutrients, may overwhelm the mitochondrial respiratory chain, leading to mitochondrial dysfunction and cell apoptosis [2]. The vicious circle of disrupted cellular energy homeostasis and resulting lipid accumulation, paired with increased concentrations of ROS, promotes the development of insulin resistance and local inflammation [2,3]. Such tissue inflammation as well as immigration of activated immune cells into organs as liver and adipose tissue caused by diet-induced obesity or other dietary overload has already been investigated [4–7]. To execute their specific role, functional mitochondria are essential for every cell. Focusing on energy homeostasis in states of altered body weight and lipid accumulation, liver and adipose tissue are highly affected by mitochondrial dysfunction [8]. Correlations of obesity and mitochondrial dysfunction in liver and white adipose tissue (WAT) have been described [9–11]. In the liver, this can lead to non-alcoholic fatty liver (NAFLD) and non-alcoholic steatohepatitis (NASH) [12–16]. In early stages of obesity, with or without fatty liver, mitochondria can still adapt and increase cellular respiration and oxidative function [17]. In case of extensive changes in the liver, as inflammation and fibrosis in NASH, mitochondrial function is decreased together with reduced ATP and increased ROS production [17]. In WAT, obesity has been shown to directly induce impaired mitochondrial function [18,19]. Cellular mitochondrial dysfunction is currently the focus of extensive research in numerous diseases like atherosclerosis, cancer, obesity, fatty liver, and NASH [1,2,8,16,17,20–23]. Thus, a sound understanding of organ- and tissue-specific mitochondrial function and dysfunction in various (pathophysiological) conditions can lay a foundation for therapeutic approaches to those diseases. However, functional analysis of mitochondria within tissues remains a challenge.

Initially, isolated mitochondria were used to estimate mitochondrial function, followed by studies on isolated cells already providing more comprehensive data. Nevertheless, the isolation process and subsequent culture conditions of those cells can induce substantial (metabolic) changes, even within the mitochondria [24]. The analysis of oxygen

[1]Department of Endocrinology and Metabolism, Charité—Universitätsmedizin Berlin, corporate member of Freie Universität Berlin and Humboldt-Universität zu Berlin, Germany [2]DZHK (German Centre for Cardiovascular Research), Partner Site Berlin, Germany [3]German Federal Institute for Risk Assessment (BfR), German Centre for the Protection of Laboratory Animals (Bf3R), Berlin, Germany [4]Technology Platform for Electron Microscopy at the Max Delbrück Center for Molecular Medicine in the Helmholtz Association (MDC), Berlin, Germany

*Corresponding author. Department of Endocrinology and Metabolism, Charité—Universitätsmedizin Berlin, Luisenstraße 13a, 10117 Berlin, Germany. E-mail: joachim.spranger@charite.de (J. Spranger).

Received April 30, 2022 • Revision received July 15, 2022 • Accepted July 26, 2022 • Available online 6 August 2022

https://doi.org/10.1016/j.molmet.2022.101563

Abbreviations

Acaca	acetyl-CoA carboxylase 1
BAT	brown adipose tissue
Cd36	cluster of differentiation 36 (aka fatty acid translocase)
ECAR	extracellular acidification rate
eWAT	epididymal white adipose tissue
FCCP	fluoro-carbonyl cyanide phenylhydrazone
Fasn	fatty acid synthase
FFA	free fatty acids
G6pc	glucose-6-phosphatase catalytic-subunit 1
HFD	high-fat diet
HSD	high-sucrose diet
iWAT	inguinal white adipose tissue
KRBH	Krebs-Ringer-Bicarbonate-HEPES
LV	left ventricle
NASH	non-alcoholic steatohepatitis
OCR	oxygen consumption rate
Opa1	mitochondrial dynamin like GTPase
Ppara	peroxisome proliferator-activated receptor alpha
RD	regular maintenance chow
ROS	reactive oxygen species
SC	spare capacity
STD	standard-control diet
Tfam/TFAM	transcription factor A, mitochondrial
Ucp1	uncoupling protein 1
WAT	white adipose tissue
WD	western diet
XFe96	Seahorse XF96 extracellular flux analyzer

concentration within tissue samples has so far been possible using the Oroboros system, only allowing for the measurement of a very small sample number [25]. Recently, Neville and colleagues established a promising technique to evaluate mitochondrial function in isolated drosophila brain tissue *ex vivo* via measuring oxygen consumption on a Seahorse flux analyzer [26].

The aim of our study was to investigate mitochondrial function in metabolically relevant murine tissues challenged by different metabolic stressors, such as diet, aging and fasting. Hence, we adapted the aforementioned method to directly screen oxygen consumption rate (OCR) and extracellular acidification rate (ECAR) of various tissue biopsies *ex vivo* in a 96-well throughput to examine mitochondrial function-related characteristics of liver, brown and white adipose, pancreatic and cardiac tissue.

2. MATERIAL AND METHODS

2.1. Animal experiments

All animal experiments were approved by institutional and national authorities (Landesamt für Gesundheit und Soziales, Berlin, Germany) in several applications (G0242/15, T0180/16, G0028/17, G0219/17, T-CH0019/21) and conducted in compliance with the institution's ethical guidelines and in accordance with EU Directive 10/63/EU, as well as in line with the ARRIVE guidelines.

All mice were maintained in individually ventilated cages (2-3 mice/cage) environmentally controlled with a 12 h light/dark cycle and *ad libitum* access to diet and water. All studies were conducted using male mice with a C57BL/6J background, except for one study, in which C57BL/6N were analyzed. Mice were purchased from Charles River or bred in-house, transferred into the animal facility and acclimatized for minimum one week prior to specific interventions.

2.2. Diets

To induce metabolic stress, dietary interventions started at the age of 6 weeks. Mice were fed either a standard-control diet (STD), a high-sucrose diet (HSD), a high-fat diet (HFD), or a western diet (WD) consisting of a HFD supplemented with 6% sucrose in the drinking water for 12 weeks. All were purchased from Ssniff Spezialdiäten and their nutritional composition is depicted in Table 1 (and details in Supplementary Tables S1—4). For maturing under metabolic stress, 5-month-old mice were fed a HFD for 12 weeks and the "aging group" aged for 2 years on a regular maintenance chow (RD). Old mice of the aging group were randomly assigned to a fed group with *ad libitum* access to food and to a fasted group without access to diet overnight. A detailed overview of cohort sizes and experiment assignment is listed in Supplementary Table S5.

2.3. Body composition

During dietary intervention, all animals were scored and weighed weekly. Fat and lean mass were assessed by ^{1}H-magnetic resonance spectroscopy using a Minispec LF50 Body Composition Analyzer (Bruker), time-points are indicated in graphs.

2.4. Sample preparation

All experiments were consistently conducted according to standardized protocols at same time of the day. Terminally, mice were sacrificed and first the organs relevant for tissue measurements were quickly extracted and weighed. Biopsies were immediately taken for assessment of mitochondrial function. One mouse per intervention group within an experiment was sacrificed simultaneously to assure equal conditions. The tissue biopsies were prepared with the help of punches (Biopsy punch, plunger type; KAI medical) and different diameter from 1 to 2 mm (Figure 1C and Supplementary Fig. S1A) were tested in order to identify the appropriate punch size for each tissue. To ensure reproducibility and comparability, all samples of one organ were prepared identical (liver: 1 mm, left ventricle (LV): 1 mm, pancreas: 1 mm, epididymal white adipose tissue (eWAT): 1.5 mm, brown adipose tissue (BAT): 1.5 mm), also in terms of preparation order and time. Identical for all experiments, freshly produced biopsies were placed in the 96-well plate, one biopsy per well and 3—5 wells (replicates) per tissue per mouse, and kept in assay medium (DMEM5030, Sigma) at 37 °C with 10 mM glucose and 2 mM glutamine until the measurement (see standardized lab protocol in Supplementary Table S6). Based on a publication by Neville and

Table 1 — Nutritional composition of used mouse diets purchased from Ssniff.

Name	Maintenance (RD)	Control (STD)	High-Sucrose (HSD)	High-Fat (HFD)
Number	V1124-300	S8090-E050	S8090-E052	E15742
Protein (kcal%)	24	20	20	20
Carbohydrate (kcal%)	67	65	65	20
Sucrose (kcal%)		7	58	9.4
Fat (kcal%)	9	15	15	60
Total (kcal%)	100	100	100	100
Metabolizable energy (kcal/kg)	3225	3680	3752	5150
Metabolizable energy (MJ/kg)	13.5	15.4	15.7	21.6

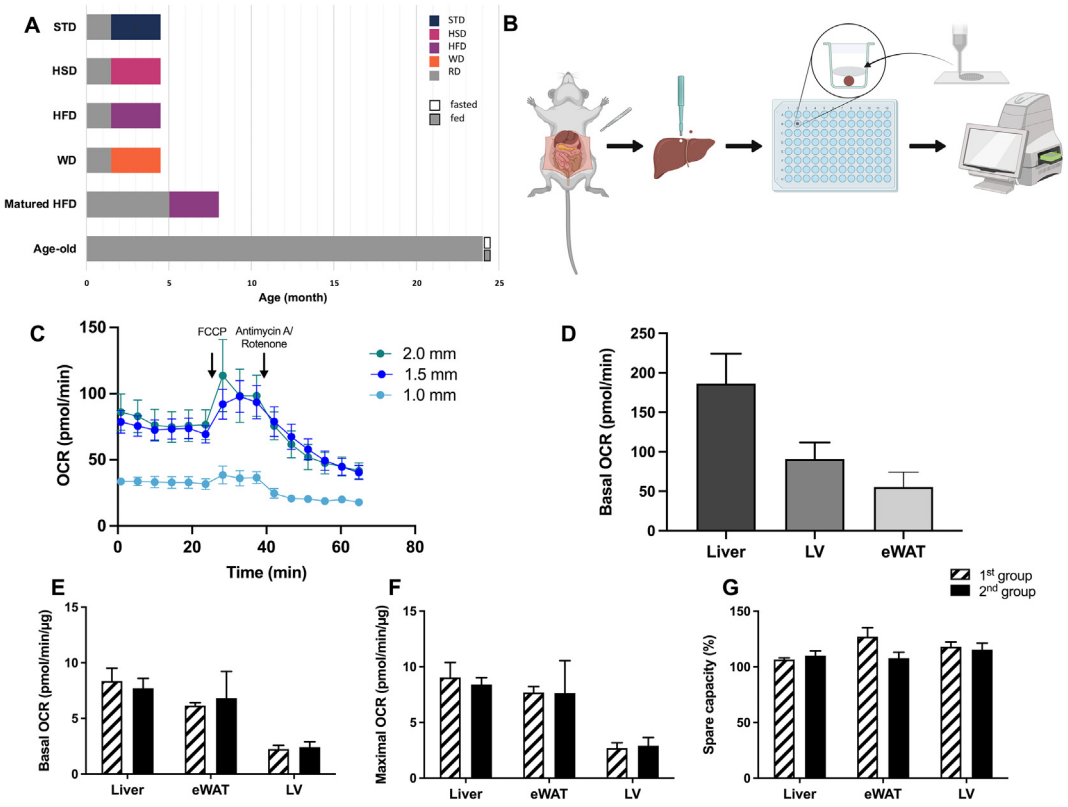

Figure 1: Experimental setup and reproducibility assessment. Comparative baseline oxygen consumption rate (OCR) measurements in tissue biopsies of naïve, young adult male BL/6J mice in two independent groups (1st and 2nd group). (A) Schematic of dietary intervention, aging and experimental procedures. (B) Overview of the experimental setup. (C) Evaluation of 1.0, 1.5, and 2.0 mm punch sizes for measurement of oxygen consumption rate (OCR) in epididymal white adipose tissue (eWAT). (D) Basal OCR of liver, left ventricle (LV) and epididymal white adipose tissue (eWAT). (E) Basal OCR per µg protein in liver, eWAT and LV. (F) Maximal OCR after FCCP application in liver, eWAT and LV. (G) Spare capacity (SC) in liver, eWAT and LV. Statistical significance was calculated using a two-tailed unpaired Student *t* test (E–G). Data represent mean ± SEM. n = 8 (C), n = 5 (D); n = 7 1st, n = 5 2nd group (E–G). HFD, high-fat diet; HSD, high-sucrose diet; RD, regular maintenance chow; STD, standard-control diet; WD, western diet.

colleagues [26], micro-restrainer were used to keep tissue biopsies in position in the well of the cell culture microplate during measurements. The 3D printing process of those micro-restrainer is described in 2.5. After biopsy pieces were taken, additional tissue samples were immediately harvested and prepared for further experiments, e.g. lipolysis, microscopy etc. or snap-frozen for storage, RNA and protein extraction.

2.5. Micro-restrainer

To overcome the limitations of production for the micro-restrainer described by Neville at al. [26], SLA (stereolithography) 3D printing technology was utilized to enable rapid production of respective devices. Information about the micro-restrainer dimension was kindly provided by Neville and colleagues. A simplified model was prepared by Computer Aided Design (Supplementary Figs. S2A and B) and a printing file was created using a proprietary slicing software, provided by the 3D printer manufacturer (Anycubic). Printing was done in highest resolution (25 µm) with an Anycubic Photon 3D printer using UV-sensitive resin type "Basic" (green, Anycubic). Subsequently to the printing process, micro-restrainer were washed with isopropanol in an ultrasonic bath and further cured by UV-radiation. Upon use, micro-restrainer were cut from their printing support, checked for integrity, and rinsed for at least 48 h in dH_2O. To ensure that the material of the micro-restrainer does not interfere with the OCR measurements, different printing resins were evaluated with primary hepatocytes in seahorse measurements in advance.

2.6. Oxygen consumption and extracellular acidification rate

Real-time OCR and ECAR were measured using a Seahorse XFe96 extracellular flux analyzer (XFe96; Agilent, Germany) at 37 °C. After assessment of the basal OCR with a minimum recording of 6 cycles [27], 5 µM FCCP (Sigma) were injected for 3 cycles as uncoupler to measure the maximal OCR and finally 2.5 µM antimycin A (Sigma) and 2.5 µM rotenone (Sigma) were injected for another 6 cycles to inhibit the respiratory chain. Titration experiments were carried out to assess the appropriate concentrations of FCCP injection (Supplementary Figs. S1B and C). After evaluation of all test runs from different organs, the standardized lab protocol used for all tissues was established for the seahorse measurements (Supplementary Table S6). The spare capacity (SC) of tissues was calculated as the difference between maximal and basal OCR and indicates the adaptability of the organ towards situations of increased ATP demand or metabolic stress. ECAR measurements monitor the medium acidification as change of pH by released protons, e.g. generated during glucose catabolism.

For normalization, each biopsy was mechanically disrupted in homogenization buffer (250 mM sucrose, 20 mM HEPES, 1 mM EDTA, pH 7.4), and lysates were exclusively used for Micro BCA Protein Assay Kit (ThermoFisher) determination to normalize seahorse measurements to protein abundance per well.

2.7. Western blot

Snap frozen tissue pieces from same mice as used for seahorse analysis were lyzed in homogenization buffer with Protease Inhibitor

(cOmplete™, Roche) and protein concentration was determined with BCA (ThermoFisher). Lysates were heated to 50°C for 5 min in Laemmli buffer with 10% β-mercaptoethanol. 15 μg of liver and eWAT or 5 μg of BAT total protein lysates were separated by SDS-PAGE gels, blotted onto nitrocellulose membranes, and blocked (5% skim milk/TBS-T). Total OXPHOS Rodent WB Antibody Cocktail (ab110413, Abcam), rabbit anti-mouse GAPDH (2118, Cell Signaling), rabbit anti-mouse TFAM (22586, proteintech), HRP-linked anti-rabbit IgG (7074, Cell Signaling) or HRP-linked anti-mouse IgG (7076, Cell Signaling) were used for detection on a ChemiDoc XRS+ (Bio-Rad) and quantified for optical density with GAPDH as loading control for each tissue using Image Lab (Bio-Rad).

2.8. qPCR

mRNA extraction and qPCR were performed as described [28]. In brief, total RNA was extracted from snap-frozen tissue samples using TRIzol (Ambion) according to the manufacturer's protocol. 1μg RNA was digested with DNase (ThermoFisher) and transcribed into cDNA via RevertAid Reverse Transcriptase (ThermoFisher). Quantitative real-time PCR was performed on a LightCycler96 (Roche) with GoTaq qPCR Master Mix (Promega) detection system. qPCR data were evaluated for relative gene expression using the $2^{-\Delta\Delta CT}$ method. Relative expression of *G6pc, Acaca, Fasn, Pparα, Cd36, Ucp1, Tfam, and, Opa1* was normalized to *18S* rRNA as housekeeping gene. Primer sequences are detailed in Supplementary Table S7.

2.9. Lipolysis assay

250 mg of STD-, HSD-fed or 500 mg of HFD- and WD-fed adipose tissue was freshly isolated after extraction pieces for punch biopsies, transferred into 37 °C KRBH+ (Krebs-Ringer-Bicarbonate-HEPES; 20 mM HEPES, 5 mM KH2PO4, 1 mM MgSO4, 1 mM CaCl2, 136 mM NaCl, 4.7 mM KCl, 1 g/l glucose, 2% BSA), minced, and digested with fresh collagenase type II (C6885, Sigma) for 30 min in a shaking water bath @ 37°C with 120 rpm disrupting tissue by pipetting every 7 min. Digested adipocytes were filtered through a 250 μm cell strainer (ThermoFisher). After 5 min for layer formation (adipocyte toplayer and sublayer buffer), buffer was withdrawn, adipocytes were washed with KRBH+ and after layer formation buffer was aspirated again. Adipocyte were appropriately adjusted with KRBH+ to the sample with lowest cell weight and adipocyte solution was plated in a 96-well plate (V-shape, Sarstedt). Triplicates were stimulated with 0, 1, 10, 25, 50 nM isoprenaline (Sigma) on a plate shaker with 300 rpm for 3.5 h at 37°C. 10 min before end, shaking was stopped to allow layer formation again and buffer was collected and stored at −80°C for analysis of free fatty acid (FFA) secretion in duplicates via NEFA-HR(2) kit (Wako).

2.10. Hepatic fat accumulation

For histology, freshly isolated tissue samples were stored in 4% Histofix (Roth) @ 4°C. Liver samples were transferred in O.C.T. Compound (Sakura) at dry ice and 6 μm sections were cryocut using a Jung Frigocut 2800E (Leica). Neutral lipids were histologically quantified using Oil-Red O (ORO) stainings of 8 sections per mouse in 10× magnification as described [29]. Mean ORO-covered area was analyzed via ImageJ (V1.48) selecting the green channel for best contrast separation with a fixed threshold from 0 to 70 to select for ORO-stained area. For quantification, all images were automatically evaluated using a macro.

Triglycerides were biochemically assessed from snap frozen liver samples as specified [30].

2.11. Transmission electron microscopy

Freshly isolated tissue samples were punched with 1 mm^3 for 3—5 times and immediately fixed by immersion with 2% (w/v) paraformaldehyde and 2.5% (v/v) glutaraldehyde in 0.1 M phosphate buffer at RT for 2 h and at 4°C overnight. Samples were transferred to 1% paraformaldehyde in 0.1 M phosphate buffer at 4°C for long-term storage and then postfixed and stained consecutively with 1% (w/v) tannic acid, 1% (v/v) osmium tetroxide, and 2% (w/v) uranylacetate at RT, dehydrated in a graded series of ethanol, and embedded in PolyBed® 812 resin (Polysciences). Ultrathin sections (60—80 nm) were made and stained with uranyl acetate and lead citrate, and examined at 80 kV with a Zeiss EM 910 electron microscope (Zeiss). Acquisition was done with a Quemesa CCD camera using iTEM software (Emsis GmbH) at 5000× magnification with a field of view of 11.2 × 7.4 μm per image. 9 independent images per mouse at different positions within the liver sections representing hepatocytes were used for evaluation and quantification of mitochondria.

2.12. Statistics

All data are presented as mean ± standard error (SEM). GraphPad Prism 9 (La Jolla) was used for statistical analyses and graphs. Statistical significance was considered with $*p \leq 0.05$, $**p \leq 0.01$, $***p \leq 0.001$. Differences were calculated using two-tailed unpaired Student's *t*-test or Mann—Whitney test and one-way ANOVA adjusted with Tukey's multiple comparisons test for post-hoc analysis or Kruskal Wallis test by ranks with Dunn's multiple comparisons test and two-way (repeated measures) ANOVA with Bonferroni multiple comparisons test. All depending on whether data passed normal distribution tests.

3. RESULTS

3.1. Oxygen consumption in tissue biopsies of naïve, young mice

The major aim of this study is to investigate changes of OCR in metabolic active tissues induced by different metabolic stressors (Figure 1A). OCR in organs and tissues has an eminent metabolic importance. However, its assessment is complicated as usually *in vivo* aspects get lost during preparation for measurements, e.g., dietary effects if explanted cells are cultured. Therefore, we developed a method, inspired by the approach of Neville and colleagues, to assess the OCR in freshly isolated organ biopsies *ex vivo,* in order to preserve tissue context, integrity and especially physiological conditions [26]. A schematic of the experimental procedure measuring OCR using tissue biopsies is illustrated in Figure 1B. Tissues are immediately removed after euthanasia, punch biopsies instantly sampled, directly placed in the 96-well plate at 37°C and held in position by a 3D printed micro-restrainer, also during measurements (Supplementary Fig. S2). To determine the appropriate tissue biopsy size, we tested different punch sizes (Figure 1C and Supplementary Fig. S1A). OCR measurements in monolayer-cultured cells, e.g., hepatocytes, adipocytes, immune cells or neurons, are well established and commonly used. As tissues with highest relevance, with respect to their cellular metabolic activity under (patho-)physiological conditions, we first tested this method using liver, epididymal white adipose tissue (eWAT) and heart tissue (left ventricle, LV) (Figure 1D). Measurements of those biopsies produced similar OCR ratios as published for the respective cell type (hepatocytes, adipocytes or cardiomyocytes) [31—33]. In addition to equal punch biopsy diameters, we assessed protein content of the biopsies for normalization to assure comparability of results from independent experiments and groups in the following.

To determine a baseline reference after the successful methodological establishment, we measured OCR in metabolic relevant organs without metabolic challenge. Consequently, a first group (1st) of naïve, young adult, male BL/6J mice were housed on a standard-control diet (STD) and OCR was measured in liver, eWAT and LV. To evaluate methodological robustness and reproducibility, the analyses were repeated in a second group (2nd) under comparable conditions (age, diet, background) three months later. Both groups exhibited similar body weight and composition (Supplementary Fig. S3). Basal OCRs of both groups was nearly identical in all three tissues (Figure 1E) indicating reproducible measurements.

After measuring basal OCR, the maximal OCR was monitored applying FCCP, an uncoupler of the respiratory chain. Thereby, the OCR increased slightly in all examined tissues (Figure 1F). Noteworthy, the stimulated OCR increase of tissue biopsies differed substantially in comparison to those observed in cell monolayers, where higher uncoupling effects occur. From basal and maximal OCR, the spare capacity (SC) was calculated, which represents the adaptive capacity of tissue in situations of increased ATP demand or metabolic stress [34]. Interestingly, LV and eWAT showed a higher SC than liver (Figure 1G).

In summary, our tissue OCR baseline measurements from liver, eWAT and LV showed comparable basal OCR results as cell monolayers and provided reliable data without environmental and time-related interferences.

Furthermore, we examined whether the genetic strain background difference between BL/6J and BL/6N specifically influences OCR but observed no differences under comparable conditions. Similar basal and maximal OCR as well as SC were measured in liver and eWAT biopsies of naïve mice without stimulation (Supplementary Fig. S4). In response to our findings, we proceeded with obesity-prone BL/6J mice to investigate the impact of metabolic stressors on OCR.

3.2. Dietary interventions in young mice induced marginal effects on OCR but reduced OXPHOS complexes in eWAT

After the assessment of baseline conditions, we investigated the impact of different key nutrients on mitochondrial respiration. Dietary interventions such as high-fat diet (HFD) and western diet (WD) are frequently used models to induce metabolic stress also resulting in weight gain, fat accumulation, insulin resistance, inflammation and/or fibrosis in mice. Therefore, a study was set up feeding 6-week-old male mice either a STD as control, a HFD, a high-sucrose diet (HSD), or a WD for 12 weeks. As expected, mice on HFD and WD exhibited a significantly increased body weight after 8 and 7 weeks of intervention, respectively (Figure 2A). No difference was observed between HSD and STD or between HFD and WD. Moreover, fat mass gain was significantly higher during HFD and WD, without differences in lean mass and also similar between STD and HSD (Figure 2B and Supplementary Fig. S5A). After the dietary intervention, mice were sacrificed to harvest tissue biopsies from various organs for assessment of their mitochondrial function. HFD increased eWAT weight ($p = 0.008$) and WD eWAT and brown adipose tissue (BAT) weight ($p = 0.030$ and $p = 0.025$, respectively), whereas the weights of pancreas, kidney, spleen and heart but, unexpectedly, also liver showed no significant differences (Figure 2C and Supplementary Fig. S5B). Surprisingly, we observed no significant changes of OCR in liver and eWAT (Figure 2D–I), as well as in pancreatic and LV tissue between dietary groups (data not shown). However, BAT exhibited an elevated basal OCR after HSD in comparison to HFD ($p = 0.042$; Figure 2J). A similar trend was observed for maximal OCR in BAT, however, this finding missed statistical significance ($p = 0.056$, Figure 2K) and SC did not differ between groups (Figure 2L).

To examine whether the different diets affected the composition of mitochondria, the protein abundance of different representative respiratory chain complex proteins was assessed by western blot examinations of liver, eWAT and BAT. The data corroborated our OCR analyses and revealed no differences of mitochondrial complexes in liver between groups (Supplementary Fig. S5D). However, in eWAT a decreased complex II and complex IV were observed in all dietary groups compared to STD ($p \leq 0.001$; Figure 2N). Furthermore, complex I was reduced in WD ($p = 0.007$; Figure 2N). Similar tendencies were found in the OCR measurements, however, did not reach statistical significance (Figure 2G and H). Interestingly, in BAT we observed an increase of complex IV protein in HSD and WD-fed and additionally an increased complex III in WD-fed mice (both $p < 0.001$; Figure 2P). Our mitochondrial respiration measurements in BAT showed a similar trend in mice fed the sucrose-containing diets, HSD and WD (Figure 2J and K). To detect structural adjustments in response to the different diets, we assessed the mitochondrial transcription factor A (TFAM) and mitochondrial dynamin-like GTPase (OPA1) as estimation for regulation and amount of mitochondrial DNA. Expression of *Tfam* and *Opa1* in eWAT were not upregulated and TFAM abundance did not differ in eWAT and BAT between dietary groups but was reduced in liver of HFD- and WD-fed mice (both $p = 0.02$; Figure 2N, P and Supplementary Figs. S5D and 5E). Moreover, several glucose and lipid metabolism genes remained unchanged in liver (Supplementary Figs. S5F–5J).

In summary, the three-month dietary interventions at young age affected only marginally tissue OCR measurements, however, we observed some structural adaptations in liver, eWAT and BAT.

3.3. Maturing during metabolic stress reduced hepatic metabolic flexibility but increased OCR in eWAT and BAT

A common hypothesis in aging is the free radical theory, which proposes that aging is caused by accumulation of ROS leading to mitochondrial DNA mutations [35]. As mitochondria are a major source of intracellular ROS, they presumably play a key role in the aging process [36]. Since we observed only minor dietary-induced effects on mitochondrial respiration in young adult mice, we combined HFD-feeding with advanced maturation (30 weeks). The matured group was compared to the young adult group (18 weeks), both fed HFD for 12 weeks. The matured mice not only gained significantly higher body weight but also developed more fat mass, while maintaining their level of lean mass ($p = 0.013$ and $p = 0.019$; Figure 3A and B). Additionally, liver, eWAT, and BAT weight was increased, whereas weight of heart and other organs did not differ ($p = 0.023$, $p = 0.031$, $p = 0.037$; Figure 3C and Supplementary Fig. S6A). Although liver weight was considerably elevated, no change in hepatic OCR could be observed (Figure 3D and E). Contrary to young mice, the SC of matured mice was significantly lower indicating a loss of metabolic flexibility towards uncoupling conditions under maturing in combination with metabolic stress ($p < 0.001$; Figure 3F). Adipose tissues revealed an increased OCR in eWAT and BAT ($p = 0.007$ and $p = 0.008$; Figure 3G and H and $p = 0.001$ and $p = 0.011$, respectively; Figure 3J and K). Consequently, eWAT and BAT of matured HFD-fed mice showed a higher energy turnover. The SC of eWAT and BAT did not differ between both groups (Figure 3I, L). Finally, our measurements did not reveal any difference for OCR or SC in LV between young and matured mice exposed to metabolic stress (data not shown). Interestingly, western blot quantification of hepatic respiratory chain complexes revealed a

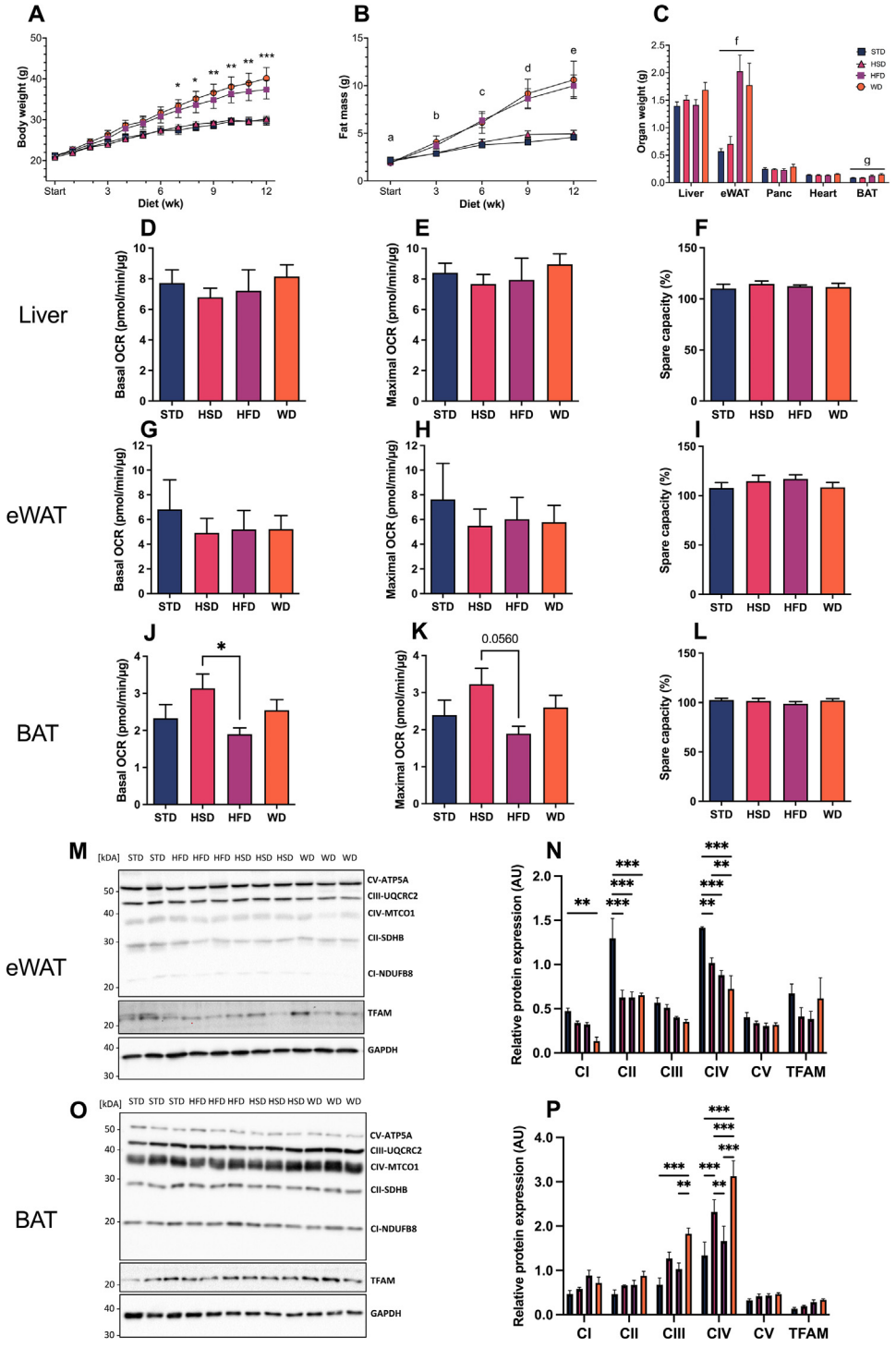

Figure 2: Evaluation of diverse dietary interventions. Body parameter, OCR, OXPHOS and TFAM in tissues during 12 weeks of standard-control (STD), high-sucrose (HSD), high-fat (HFD) or western diet (WD). (A) Weight progression. (B) Fat mass; a-c, nonsignificant (ns), d, STD vs. HFD $p = 0.001$, STD vs. WD $p = 0.0002$, STD vs. HSD ns, HSD vs. HFD $p = 0.006$, HSD vs. WD $p = 0.0011$, HFD vs. WD ns; e, STD vs. HFD $p < 0.0001$, STD vs. WD $p < 0.0001$, STD vs. HSD ns, HSD vs. HFD $p < 0.0001$, HSD vs. WD $p < 0.0001$, HFD vs. WD ns. (C) Organ weights after diet; f, STD vs. HFD $p = 0.008$, STD vs. WD $p = 0.03$, HSD vs. HFD $p = 0.011$, HSD vs. WD $p = 0.001$. g, STD vs. WD $p = 0.025$, HSD vs. WD $p = 0.0181$. (D–F) Basal (D), maximal OCR (E) and spare capacity (SC) (F) of liver. (G–I) Basal (G), maximal OCR (H) and SC (I) of epididymal white adipose tissue (eWAT). (J–L) Basal (J), maximal OCR (K) and SC (L) of brown adipose tissue (BAT). (M) Representative blot of OXPHOS complexes I–V, TFAM and GAPDH in eWAT. (N) Quantification of western blot analysis of the respiratory chain complexes and TFAM in eWAT. (O) Representative blot of OXPHOS complexes I–V, TFAM and GAPDH in BAT. (P) Quantification of western blot analysis of the respiratory chain complexes and TFAM in BAT. (N, P) Relative protein abundance of complex I (CI: NDUFB8), complex II (CII: SDHB), complex III (CIII: MTCO1), complex IV (CIV: UQCRC2), complex V (CV: ATP5A) and TFAM normalized to GAPDH (37 kDa) as loading control. $*p \leq 0.05$, $**p \leq 0.01$, $***p \leq 0.001$. Statistical significance was calculated using one-way ANOVA with Tukey's multiple comparisons test (C (tested per tissue), D, E, I, P-R) or Kruskal–Wallis test by ranks with Dunn's multiple comparisons test (F–H) or two-way ANOVA with Bonferroni multiple comparisons test (A, B, N, P). Data represent mean ± SEM. n = 5 STD, n = 6 HSD/HFD/WD (A–R). AU, arbitrary units; BAT, brown adipose tissue; eWAT, epididymal white adipose tissue; panc, pancreas; TFAM, Transcription Factor A, Mitochondrial.

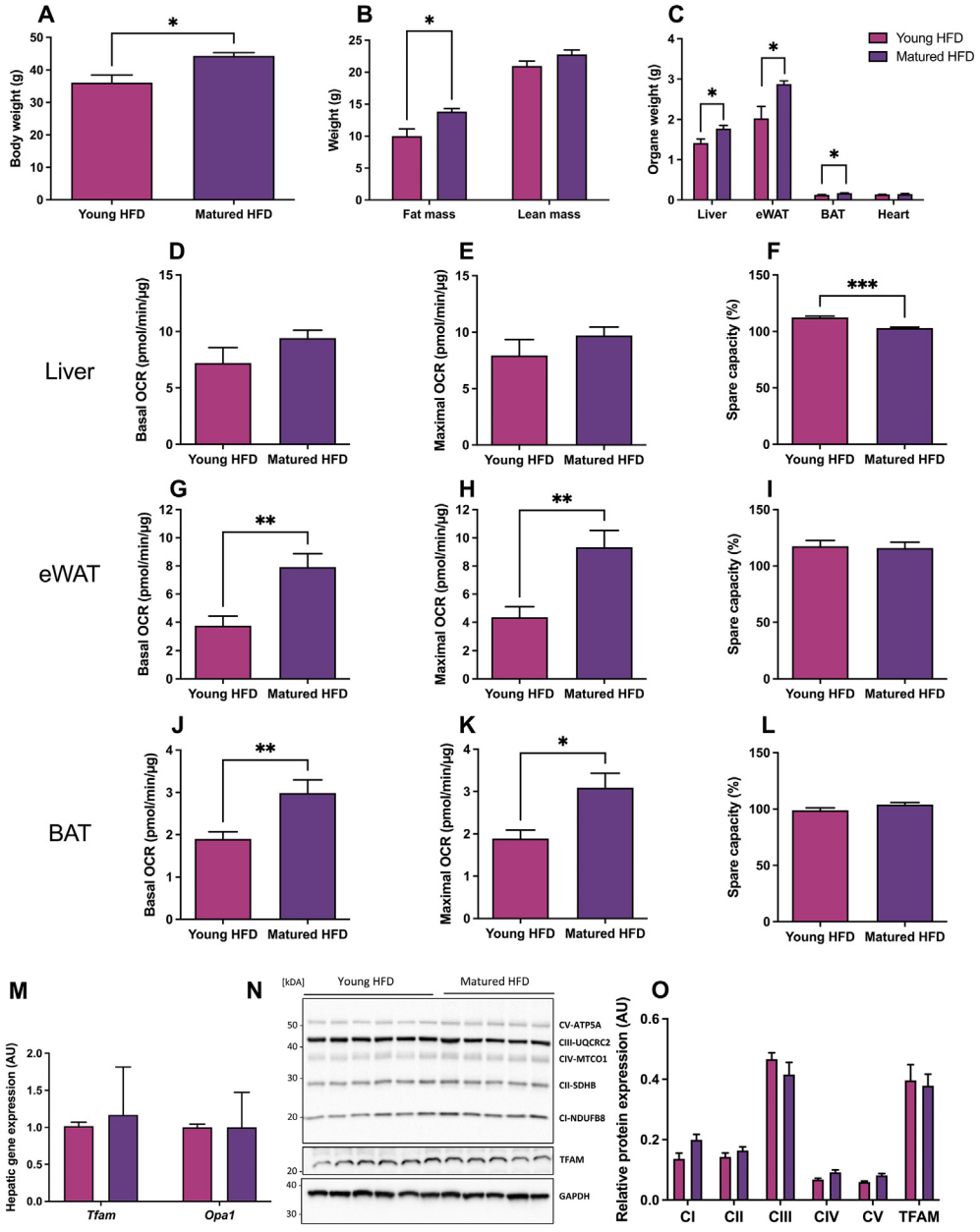

Figure 3: Maturing on high-fat diet. Body parameter, tissue OCR measurements and hepatic OXPHOS and TFAM analysis of young (18 weeks) vs. matured (30 weeks) male mice after 12 weeks of high-fat diet (HFD). (A) Body weight after 12 weeks HFD. (B) Fat mass and lean mass. (C) Final organ weights. (D—F) Basal (D), maximal OCR (E) and spare capacity (SC) (F) of liver. (G—I) Basal (G), maximal OCR (H) and SC (I) of epididymal white adipose tissue (eWAT). (J—L) Basal (J), maximal OCR (K) and SC (L) of brown adipose tissue (BAT). (M) Hepatic gene expression of *Tfam* and *Opa1*. (N) Representative blot of OXPHOS complexes I—V, TFAM and GAPDH in liver. (O) Western blot quantification of the respiratory chain complexes and TFAM in liver. Relative protein abundance of complex I (CI: NDUFB8), complex II (CII: SDHB), complex III (CIII: MTCO1), complex IV (CIV: UQCRC2), complex V (CV: ATP5A) and TFAM normalized to GAPDH (37 kDa) as loading control. $*p \leq 0.05$, $**p \leq 0.01$, $***p \leq 0.001$. Statistical significance was calculated using a two-tailed unpaired Student *t* test (A, B, C (tested per tissue), E-J, L) or Mann—Whitney test (K) or two-way ANOVA with Bonferroni multiple comparisons test (M, O). Data represent the mean ± SEM. n = 6 young HFD, n = 5 matured HFD. AU, arbitrary units; BAT, brown adipose tissue; eWAT, epididymal white adipose tissue; Opa1, mitochondrial dynamin like GTPase; TFAM, Transcription Factor A, Mitochondrial.

slight increase of complex I, IV and V in matured mice on HFD compared to young HFD mice, indicating an enhancement of mitochondrial functions, which was also observed in our OCR measurements in adipose tissue and by trend in liver (Figure 3D,G, and J), to possibly counteract an HFD-induced mitochondrial impairment (Figure 3O).

3.4. Prolonged aging increased OCR in BAT and elevated maximal OCR and SC in LV but did not influence hepatic metabolic flexibility

Since we observed stronger effects on mitochondrial respiration after maturing combined with HFD-feeding, we investigated the impact of prolonged aging in more detail. Hence, we examined mitochondrial function of various tissues from age-old mice. These mice aged for 96

weeks, were fed with a regular maintenance chow (RD; matching STD) and subsequently compared to the naïve young adult group (18 weeks) on STD.

After two years the age-old mice reached a higher body weight ($p = 0.006$; Figure 4A) with elevated fat and lean mass ($p = 0.016$ and $p = 0.001$; Figure 4B). Accordingly, their organ weights differed for liver, heart, kidney (all $p < 0.001$), pancreas ($p = 0.0014$), and furthermore showed trends for eWAT ($p = 0.053$), but not for BAT and spleen (Figure 4C and Supplementary Fig. S6B). Interestingly, we did not observe an age-mediated effect on OCR in liver and pancreatic biopsies between age-old RD and young STD mice (Figure 4D–F and data not shown). In contrast, LV of age-old mice exhibited elevated basal OCR ($p = 0.037$; Figure 4G), increased maximal OCR and a higher SC (both $p = 0.029$; Figure 4H and I). Likewise, eWAT showed an increased SC but no difference in basal or maximal OCR ($p = 0.042$; Figure 4J–L). Next, we investigated whether aging affects the mitochondrial respiration of BAT. Similarly to our findings in the matured group, we observed an increase in basal and maximal OCR, as well as an increased SC in the age-old group ($p = 0.009$, $p = 0.005$ and $p = 0.009$, respectively; Figure 4M–4O). As UCP1 (uncoupling protein

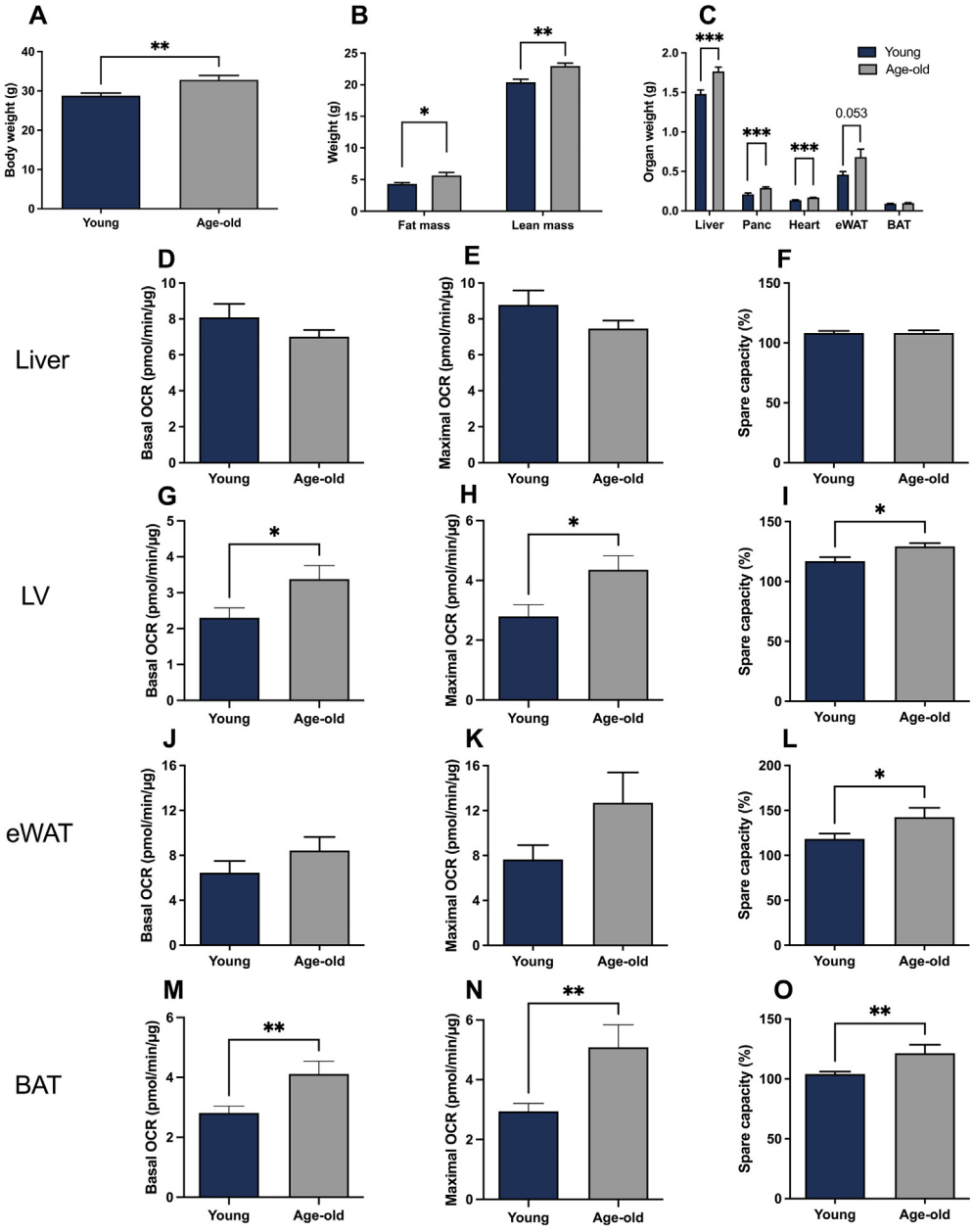

Figure 4: Analysis of prolonged aging. Body parameter and OCR in tissues of young (18 weeks) vs. age-old (2-year-old) male mice. (A) Body weight. (B) Fat mass and lean mass. (C) Organ weights after diet. (D–F) Basal (D), maximal OCR (E) and spare capacity (SC) (F) of liver. (G–I) Basal (G), maximal OCR (H) and SC (I) of left ventricle (LV). (J–L) Basal (J), maximal OCR (K) and SC (L) of epididymal white adipose tissue (eWAT). (M–O) Basal (M), maximal OCR (N) and SC (O) of brown adipose tissue (BAT). $*p \leq 0.05$, $**p \leq 0.01$, $***p \leq 0.001$. Statistical significance was calculated using a two-tailed unpaired Student *t* test (A-O, C (tested per tissue). Data represent the mean ± SEM. n = 12 (A–C); n = 12 young, n = 6 age-old (D–O). BAT, brown adipose tissue; eWAT, epididymal white adipose tissue; panc, pancreas.

1) levels decline with age it has been hypothesized that mitochondrial respiration also diminishes in BAT during the aging process [37,38]. However, we observed an increase in OCR in BAT in aged mice, while the anticipated decrease of *Ucp1* was significant in aged mice ($p = 0.0043$; Supplementary Fig. S7).

Summarizing the effects of aging, both maturing with additional metabolic stress (HFD) and prolonged aging (2 years), resulted in an increased basal and maximal OCR in BAT. Remarkably, maturing on HFD induced a reduction of hepatic metabolic flexibility and an increase of basal and maximal OCR in eWAT. The hepatic effect, however, did not occur during prolonged aging on RD.

Based on the analysis of body parameters comparing maturing HFD and aged RD mice, we deduced that HFD provoked significantly more weight and fat gain ($p < 0.001$; Figure 5A and B left). This effect was obvious within 3 months of feeding, however, could not be observed with RD within 96 weeks, reflecting the impact of HFDs. Furthermore, similar effects were also found in young HFD mice (data not shown). Likewise, there was a significantly increased fat mass as well as more eWAT and BAT in matured HFD mice with comparable lean mass ($p < 0.001$; Figure 5B right, 5C). In contrast, cardiac and renal tissues, which are known to exhibit insufficiencies in aging humans, showed a higher weight in age-old mice ($p = 0.037$ and $p = 0.041$; Figure 5C). Fascinatingly, liver weight did not differ between both groups (Figure 5C), but hepatic metabolic flexibility was impaired after HFD (Figure 3F), whereas aging per se showed no significant effect on metabolic flexibility (Figure 4F). In order to further specify the impact of high-fat feeding on liver, we measured hepatic triglyceride content and observed a tenfold increase under HFD ($p < 0.001$, Figure 5D). Additionally, histological quantifications of liver sections staining for neutral lipids using Oil-Red O (ORO, Figure 5E) revealed that aged mice barely exhibited lipid accumulation compared to HFD-fed mice which showed an extensive hepatic fat amount ($p < 0.001$, Figure 5F). In summary, this confirms the dramatic effect of HFD by demonstrating a fatty degeneration of liver tissue already within 12 weeks of HFD compared to 2 years on RD.

3.5. Fasting boosts hepatic and pancreatic OCR

Finally, we investigated the impact of fasting, as a short-term extreme metabolic stressor, on mitochondrial function. Since glucagon treatment can increase basal and maximal hepatic respiration, we and others assumed that fasting might enhance hepatic mitochondrial respiration due to increased glucagon levels [39–42]. Therefore, a second group of age-old mice was fasted overnight before measuring their OCR to identify whether their metabolic flexibility is altered to counteract aging-related changes. As anticipated, the fasting group had slightly lower body weight with reduced fat but similar lean mass ($p = 0.052$ and $p = 0.004$; Figure 6A and B). Interestingly, mice of the fasting group exhibited lower liver and pancreas weights ($p < 0.0001$ and $p = 0.011$; Figure 6C). Other organ weights did not differ (Figure 6C and Supplementary Fig. S6C). In line with our hypothesis, hepatic basal and maximal OCR was increased after fasting ($p < 0.005$, $p = 0.027$; Figure 6D and E), whereas fed mice had a higher SC ($p = 0.003$; Figure 6F), implying a descending metabolic flexibility due to a lack of adaptation in fasted livers. For pancreatic

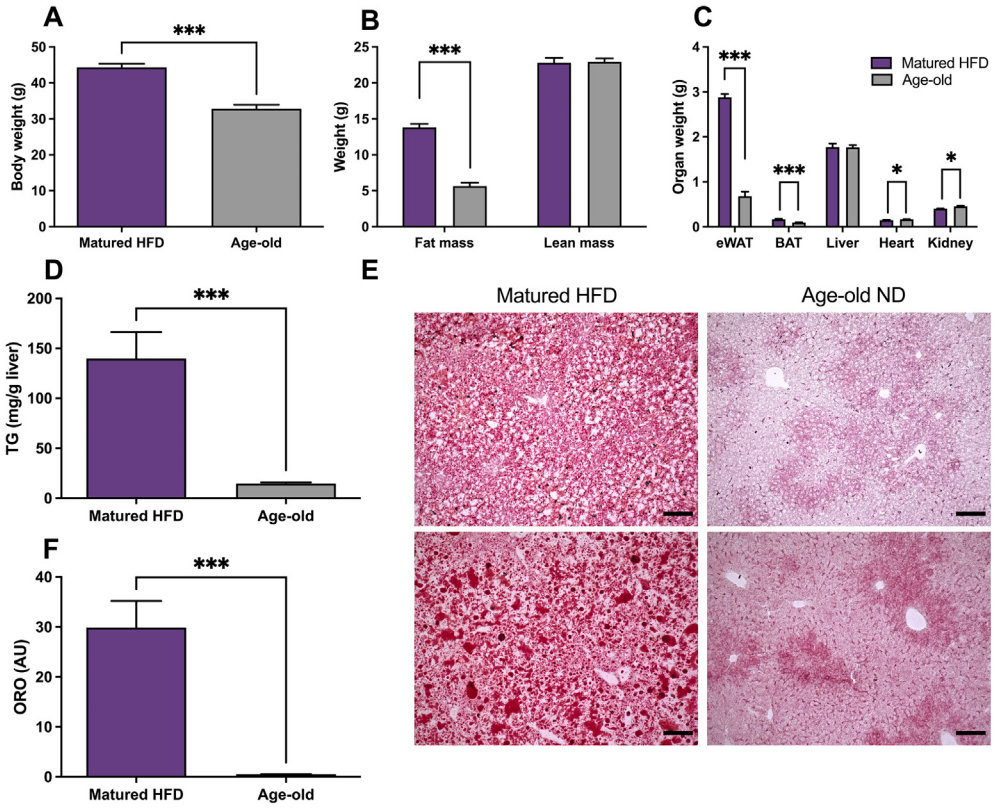

Figure 5: Comparison of maturing on HFD and prolonged aging. Body parameter and liver histology in matured mice (30 weeks) on HFD vs. age-old (2-year-old) male mice. (A) Body weight. (B) Fat mass and lean mass. (C) Organ weights after diet. (D) Hepatic triglyceride (TG) concentration of both groups. (E) Representative images of Oil-red O-stained (ORO) liver sections of mice matured on HFD (left) and age-old mice on ND (right). Black scale bars, 150 μm; magnification is 10×. (F) Quantification of hepatic ORO stainings (as in E).*$p \leq 0.05$, **$p \leq 0.01$, ***$p \leq 0.001$. Statistical significance was calculated using a two-tailed unpaired Student *t* test (A-C (tested per tissue), D, F). Data represent the mean ± SEM. n = 12 age-old, n = 5 matured HFD (A–C); n = 6 (D, F). AU, arbitrary units; BAT, brown adipose tissue; eWAT, epididymal white adipose tissue; ND, normal diet.

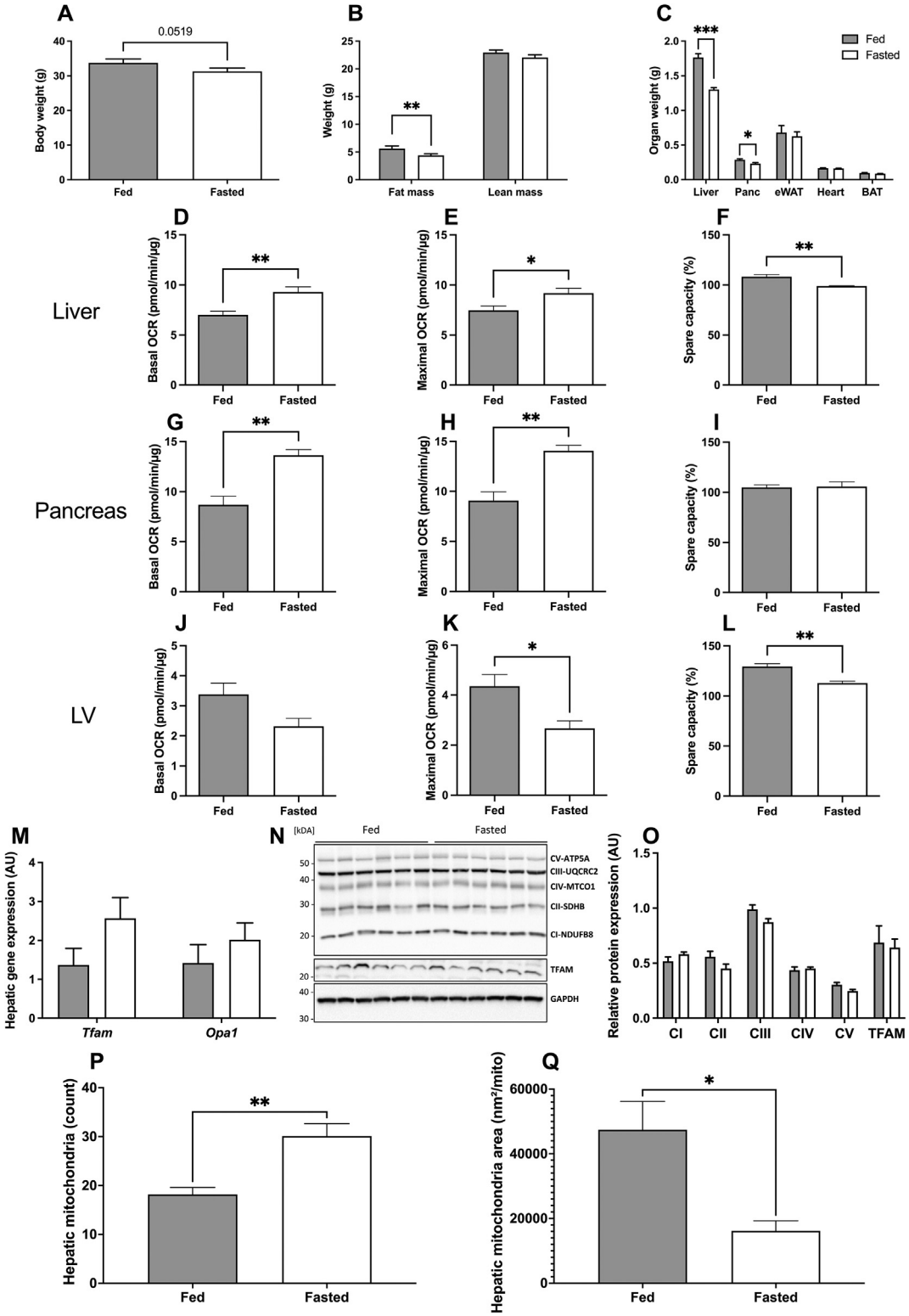

Figure 6: Effects of short-term fasting. Body parameter, OCR measurements and hepatic analyses of fed vs. overnight fasted male mice. (A) Body weight. (B) Fat mass and lean mass. (C) Organ weights. (D–F) Basal (D), maximal OCR (E) and spare capacity (SC) (F) of liver. (G–I) Basal, maximal OCR and SC of pancreas. (J–L) Basal (J), maximal OCR (K) and SC (L) of left ventricle (LV). (M) Hepatic gene expression of *Tfam* and *Opa1*. (N) Representative blot of OXPHOS complexes I–V, TFAM and GAPDH in liver. (O) Western blot quantification of the respiratory chain complexes in liver. Relative protein abundance of complex I (CI: NDUFB8), complex II (CII: SDHB), complex III (CIII: MTCO1), complex IV (CIV: UQCRC2), complex V (CV: ATP5A) and TFAM normalized to GAPDH (37 kDa) as loading control. (P) Evaluation of electron microscopic analysis of mitochondrial count within hepatocytes. (Q) Calculation of mean area per mitochondrion. $*p \leq 0.05$, $**p \leq 0.01$, $***p \leq 0.001$. Statistical significance was calculated using a two-tailed unpaired Student *t* test (B (lean mass), C (liver, heart, eWAT, Panc), D-L, P, Q) or Mann–Whitney test (A, B (fat mass), C (BAT)) or two-way ANOVA with Bonferroni multiple comparisons test (M, O). Data represent the mean ± SEM. n = 12 (A, B, C); n = 6 (D–O); n = 4 (P, Q). AU, arbitrary units; BAT, brown adipose tissue; eWAT, epididymal white adipose tissue; mito, mitochondrion; Opa1, mitochondrial dynamin like GTPase; panc, pancreas; TFAM, Transcription Factor A, Mitochondrial.

tissue, we also theorized an increased OCR representing an impairment in the respiratory chain due to fasting. Indeed, pancreatic basal and maximal OCR were elevated in fasted mice (both $p = 0.001$; Figure 6G and H), however SC did not differ (Figure 6I). Measuring LV OCR showed a similar basal OCR, however, a decrease of maximal OCR and SC in fasted mice ($p = 0.018$, $p = 0.001$; Figure 6J–L). This resembles our observations in SC in hepatic tissue.

Finally, we compared brown and epididymal WAT depots as energy sources, especially important during fasting. While we did not see any OCR changes in BAT (data not shown), a significantly lower SC in fasted eWAT could be observed ($p = 0.040$; Supplementary Fig. S8A). Summarizing the OCR data, we observed a fasting induced upregulation of OCR in liver and pancreas in our tissue measurements. Interestingly, the same trend was detected in hepatic *Tfam* and *Opa1* expression already induced by 16 h fasting (Figure 6M). Though, this did not (yet) affect TFAM abundance or the composition of respiratory complexes (Figure 6O). However, evaluating hepatocytes using transmission electron microscopy (Supplementary Fig. S8B), we revealed a strongly increased amount of mitochondria in hepatocytes of fasted mice ($p = 0.006$; Figure 6P). In contrast, the mitochondrial area was significantly reduced ($p = 0.015$; Figure 6Q), but apart from that, we did not discover obvious structural differences (data not shown).

In conclusion, our findings suggest that fasting induces enhanced mitochondrial respiration and a decrease in organ weight in energy producing tissues, such as liver and pancreas, but also a loss of metabolic flexibility in liver, eWAT, and LV, hence reflecting a lack of energy resources during fasting. Thus, these fasting-mediated effects, also observed using electron microscopy analysis, could already be assessed by our tissue OCR measurements.

3.6. Extracellular acidification rate indicates the lipolytic activity of adipose tissue

In addition to the oxygen consumption, we also evaluated ECAR monitoring as estimation of pH change by proton release. Our ECAR data predominantly correlated with the OCR results. Interestingly, in eWAT OCR and ECAR measurements appear to diverge for diets (Figure 7A, for OCR see Figure 2G). During adipocyte lipolysis, the FFA release is presumably accountable for medium acidification [33,43]. Therefore, we investigated isoprenaline-induced lipolysis of primary adipocytes with regard to ECAR. Indeed, adipocytes of HFD-fed mice showed a lower isoprenaline-stimulated FFA release (Figure 7B). In the absence of metabolic stress, adipose tissue ECAR remained unchanged comparing young and age-old mice (data not shown). However, challenging young and matured mice by HFD revealed an obvious difference in ECAR with a strong elevation in matured mice ($p = 0.0001$; Figure 7C). In contrast to a similar OCR during fasting, we observed an increased ECAR in eWAT ($p = 0.021$; Figure 7D). Consistently, adipocytes from fasted mice exhibited an increased isoprenaline-stimulated lipolytic activity ($p < 0.018$; Figure 7E). In summary, we also observed that our ECAR measurements were not providing adequately information about the glycolytic rate, as already described, but rather could be used as an estimate of lipolytic capacity of adipose tissue [33].

4. DISCUSSION

For our study we developed a novel method, inspired by recent work of Neville and colleagues measuring direct mitochondrial respiration in drosophila brains [26], enabling the analysis of OCR in small murine

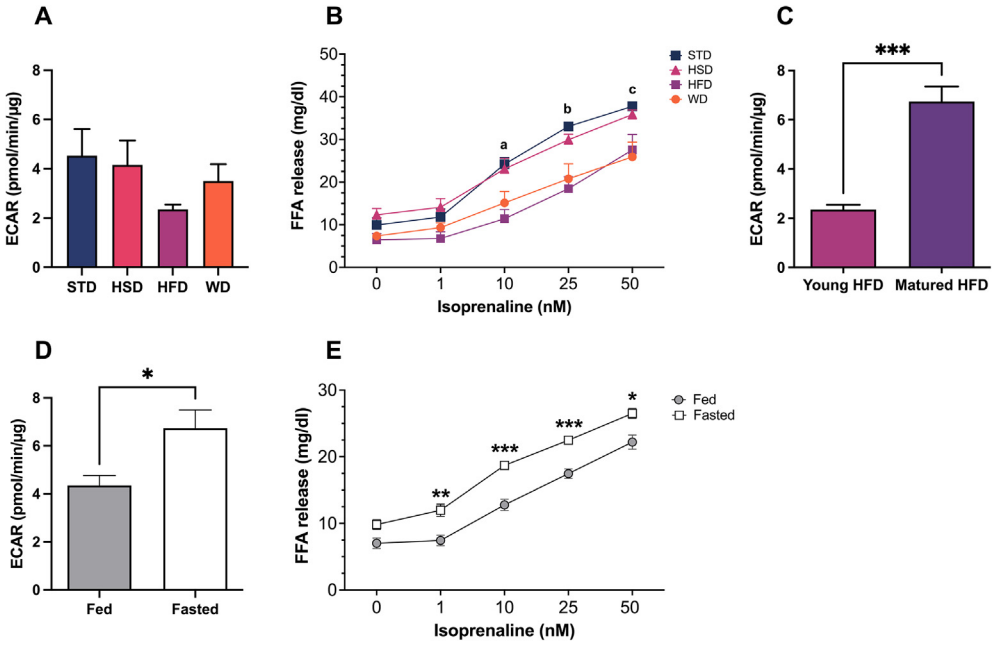

Figure 7: Extracellular acidification rate (ECAR) and lipolysis. (A) ECAR of epididymal white adipose tissue (eWAT) after 12 weeks of standard-control (STD), high-sucrose (HSD), high-fat (HFD) or western diet (WD). (B) Lipolysis after 12 weeks of STD, HSD, HFD or WD in adipose tissue. a, STD vs. HFD $p < 0.001$, STD vs. WD $p = 0.03$, STD vs. HSD ns, HSD vs. HFD $p = 0.001$, HSD vs. WD ns, HFD vs. WD ns; b, STD vs. HFD $p < 0.001$, STD vs. WD $p = 0.001$, STD vs. HSD ns, HSD vs. HFD $p = 0.002$, HSD vs. WD $p = 0.02$, HFD vs. WD ns; c, STD vs. HFD $p = 0.01$, STD vs. WD $p = 0.002$, STD vs. HSD ns, HSD vs. HFD $p = 0.04$, HSD vs. WD $p = 0.008$, HFD vs. WD ns. (C) ECAR of eWAT of young HFD and matured HFD male mice. (D) ECAR of eWAT of overnight fasted and fed male mice. (E) Lipolysis in adipose tissue of overnight fasted and fed male mice. $*p \leq 0.05$, $**p \leq 0.01$, $***p \leq 0.001$. Statistical significance was calculated using Kruskal–Wallis test by ranks with Dunn's multiple comparisons test (A) or two-way ANOVA with Bonferroni multiple comparisons test (B, E) or a two-tailed unpaired Student *t* test (C, D). Data represent mean ± SEM. n = 5 STD and matured HFD, n = 6 HSD/HFD/WD, young HFD, fasted, fed (A–D). n = 12 fasted, fed (E). FFA, free fatty acids. Tables.

tissue biopsies. An optimized protocol and improved production of biopsy micro-restrainer using 3D printing allowed for a broad comparative study on mitochondrial function in various murine tissue biopsies in the 96-well seahorse format. We established these measurements for liver, adipose tissue (eWAT and BAT), pancreas and cardiac muscle (LV). Compared to previous research in cell cultures, this procedure has the methodological advantage of analyzing the mitochondrial function in tissues *ex vivo*, while preserving tissue complexity, microenvironment and intact cell interactions of different cell clusters, e.g., immune, storage cells. *Ex vivo*, the presence of several cell types and the paracrine communication between different cells equates to a more physiological representation of the organ function. Using FCCP in our tissue measurements, we observed its uncoupling effect as in cultured cells, although with different kinetics and amplitude. The reduction of the uncoupling effect might result from the fact that FCCP cannot reach mitochondria within tissues to the same extent as in cells, due to necessary tissue diffusion. However, since we worked with identical tissue punches in each tissue, we assume that FCCP was absorbed equally in each biopsy and, thus, relative comparability within the same organ should be given. Since absorption processes of applied inhibitors, antimycin A and rotenone, in tissue biopsies were not comparable to cell monolayers, protocols of inhibitor injection will need further refinement and adaption in future studies.

We deployed the adapted tissue OCR measurements to investigate the impact of important metabolic stressors on mitochondrial function. In summary, we revealed only mild dietary effects (HFD and WD) on mitochondrial respiration in young mice, which may still be compensated by physiological counter-regulations. In contrast to young mice, HFD in matured mice lowered hepatic metabolic flexibility, while increasing OCR in eWAT and BAT. Remarkably, such a reduction of hepatic metabolic flexibility was not caused by 2 years aging without additional metabolic stress (RD). The aging process instead increased OCR in BAT. Ultimately, the metabolic stressor fasting decreased liver and pancreas weight while boosting their OCR. Moreover, fasting led to a reduction of SC and, thus, to a declined adaptability towards situations of increased ATP demand in liver, eWAT, and LV.

We observed no major effects, only trends, on liver and eWAT OCR after 12 weeks dietary interventions starting at adolescence. Likewise, Cummins and colleagues showed no significant impact of a 6-week HFD on mitochondrial function in WAT but revealed a reduced mitochondrial respiration by trend [44]. Both works exhibit comparable similar tendencies. Unlike to OCR and in line with Cummins, we detected a reduction of some respiratory chain complexes in eWAT after HFD [44]. Interestingly, this reduction was also observed under HSD and WD. Thus, it seems that mitochondria of young adult mice adapt more flexibly to metabolic stress despite reduced respiratory chain complexes. Furthermore, chronic HSD feeding can elevate *Ucp1* expression in BAT and, with it, energy expenditure in mice [45–48]. Our findings might be able to explain how UCP1-dependent upregulation of mitochondrial OCR increases energy expenditure via respiratory chain complex IV in BAT after HSD. The increased OCR seems to be induced by an elevated mitochondrial uncoupling due to a higher *Ucp1* expression and may explain why sucrose alone does not elevate body weight. Interestingly, this effect was not only induced by HSD but the same tendency in OCR as well as a significant elevation of respiratory chain complexes III and IV were evident after WD, which consists of HFD plus sucrose in drinking water. Our results suggest that dietary sucrose is a driving factor for UCP1 and thus OCR upregulation.

To investigate the influence of aging on mitochondrial respiration we examined two different aging groups, maturing under metabolic stress in terms of a 12-week HFD and prolonged aging for 2 years on RD. We observed an aging-induced increase in basal and maximal OCR in BAT in both groups. BAT plays a crucial role in thermoregulation by thermogenesis, the enhancement of energy metabolism and the protection against cold exposure and obesity [49]. Various studies have already addressed improved BAT activity in long-lived animals [50–53]. Thermoregulatory processes such as vasoconstriction decline during aging [51], thus requiring the use of BAT for heat production evidenced by an increased OCR, which was also found in our study.

Furthermore, we observed that age-old mice exhibit an increased basal and maximal OCR and SC in LV. While cardiac function, especially contraction and diastolic relaxation, declines with age, more energy may be required to provide the contractile strength in cardiomyocytes and ensure sufficient blood supply [54]. Our analysis indicates that LV mitochondria adapt to the more challenging conditions by increased respiratory activity. An aging-mediated upregulation of proteins vital to mitochondrial energy metabolism has already been described [55–57]. Among others, it was observed that Cytochrome C oxidase activity, which plays an important regulatory function of mitochondrial respiration in cardiomyocytes, increased with age in cardiomyocytes of C57BL/6 mice [58–60]. In contrast, dietary intervention at young age and HFD-feeding in matured mice showed no effect on cardiac OCR. Therefore, we conclude that heart function is preserved as long as possible and direct effects of (mild) metabolic stress(ors) on the heart are mitigated, whereas the aging process inevitably impacts cardiac function and induces an upregulation of OCR to sustain cardiac output.

As opposed to metabolic stress at young age, in which mitochondria are seemingly able to adjust, HFD feeding in matured mice showed a decreased SC in liver and, therefore, a reduced hepatic metabolic flexibility. Interestingly, this reduction of hepatic metabolic adaptability was not observed after 2 years aging. Thus, it seems that an unhealthy lifestyle in adulthood has more detrimental consequences, while (prolonged) aging alone under healthy conditions does not compromise tissues to the same extent, even if there are other, age-related changes e.g., organ weight gain. This is also exemplified by the rapid lipid/triglyceride accumulation in liver after HFD, an effect which was notably absent during RD.

Finally, the short-term stressor fasting resulted in decreased liver and pancreas weight and boosted their mitochondrial respiration, induced hepatic *Tfam* and *Opa1* mRNA upregulation by trend, but did not (yet) alter protein abundance of hepatic TFAM and key respiratory chain complexes. However, analog to decreasing liver tissue (weight), we observed a reduction of mitochondria size in livers of fasted mice together with an increasing number of mitochondria, whereas they sustained the composition of the respiratory complexes during fasting. Hence, mitochondria lose size, but their number increases within fasting hepatocytes and these provide an enhanced mitochondrial respiration, as monitored in our tissue measurements. This fasting-mediated increase of hepatic and pancreatic OCR may be induced by glucagon secretion and corresponding glycogen breakdown. During fasting, pancreatic alpha cells secrete glucagon to stimulate hepatic glucose production maintaining euglycemia [61–63]. In order for this to occur, increased levels of uncoupling protein 2 are required, which in turn leads to an increased proton transport and increased net proton conductance [64]. We suppose this mechanism disrupts the respiratory chain and, thus, pancreatic OCR is enhanced, as supported by our data. Glucagon treatment has been described to elevate hepatic

respiration, however, most studies analyzed isolated mitochondria to examine the influence of glucagon or fasting on hepatic mitochondrial respiration [39–41,65–67]. In contrast, we investigated tissues of fasted mice *ex vivo* and could confirm an increased hepatic basal and maximal OCR. With our real-time OCR measurement, we were effectively able to detect the impact of such an impressive short-term stimulus on mitochondrial function. At a regulatory level, changes were already induced, presumably to adapt towards this situation. Therefore we concluded that mitochondrial capacity gets increased to ensure cellular functionality during fasting.

Interestingly, fasting reduced SC in liver, eWAT and LV, indicating a decreased metabolic flexibility to increased ATP demand, most likely due to missing energy reserves. In conclusion, we suppose that glucagon plays a central role during fasting-mediated OCR increases in liver and pancreas, not only in isolated mitochondria [39,40,65,67] but also *ex vivo* in tissue biopsies. Moreover, fasted mice did not reduce eWAT weight during the overnight phase, as one could have expected, but rather consumed liver and pancreas tissue. This utilization of liver reserves has already been described as the depletion of hepatic glycogen storages for rapid energy supply during prolonged fasting [68]. Expanding on this, we also consider the decrease of pancreatic tissue a consequence of fasting-induced glucagon secretion, although, the pancreas could also deploy exocrine fat depots as energy reserves to supply increased mitochondrial respiration. While available research is very limited on the effects of overnight fasting, Munhoz and colleagues described a reduction of pancreas and decrease islet size after 12 weeks of intermittent fasting in mice [68]. Thus, it would be of particular interest to unravel the effect of fasting in more detail.

Not only OCR is monitored using a seahorse device, but also the ECAR is recorded. We, therefore, evaluated ECAR in our tissue biopsy measurements to investigate whether these data provide additional information. We and others have noticed that ECAR is not a useful indicator of glycolysis, as almost all metabolic processes in a cell lead to changes in proton concentration and thus can influence ECAR [33,43]. However, analyzing adipose tissue, we discovered that ECAR can be considered as an estimate for the lipolytic capacity of adipocytes in terms of stimulated FFA release.

A particular limitation of this study was that the OCR data in small skeletal muscle biopsies did not provide satisfactory results on mitochondrial respiration. This was, presumably, due to physical damage to fiber and fasciae integrity caused by tissue manipulation. We aim to further investigate measurements of oxygen consumption in muscle tissue in following studies. Presently, no adequate stimuli, like contraction or motor innervation before OCR measurement could be reproduced in our approach, and hence further stimulation experiments should be carried out. As already discussed, the inhibitors showed other kinetics and were not as effective as in monolayer-cultured cells. But *ex vivo* cultured, primary cells forfeit their characteristics during cell culture. Therefore, one has to trade off, what exactly should be investigated.

In conclusion, we investigated the mitochondrial function *ex vivo* in liver, adipose tissue, pancreas and LV in detail. From a methodological stance our novel approach provides the opportunity to analyze OCR *ex vivo* under (metabolic) challenges, as well as in other tissue samples, such as human surgical material. Furthermore, optimization of the protocol and the 96-well format enables the assessment of organ-specific OCR as a species-independent, highly innovative and relevant parameter in all kind of explorative, pharmacological or even toxicological studies.

FUNDING

This work was supported by the Department of Endocrinology and Metabolism, Charité—Universitätsmedizin Berlin and Deutsches Zentrum für Herz-Kreislauf-Forschung (DZHK BER 5.4 PR/BMBF). RS was supported by a personal CSC scholarship (201808650045). AL was supported by a graduation grant of the Deutsche Diabetes Gesellschaft.

AUTHOR CONTRIBUTION

OM: Methodology, Investigation, Analysis, Visualization, Writing—original draft, review and editing. EKW: Methodology, Investigation, Writing—review. RS: Investigation, Analysis, Writing—review. JW: Investigation. AL: Investigation. KR: 3D printing, Writing—review. SK: Investigation, Analysis. JS: Resources, Funding acquisition, Writing—review and editing. SB: Conceptualization, Methodology, Investigation, Analysis, Project supervision, Resources, Funding acquisition, Writing—original draft, review and editing.

DATA AVAILABILITY

Data will be made available on request.

ACKNOWLEDGMENTS

We thank Diana Woellner, Marie-Christin Gaerz and Nadine Huckauf, Charité — Universitätsmedizin Berlin for excellent assistance with mouse and biochemical experiments. Furthermore, we thank Quin Kuettner for language editing of the revised manuscript. Moreover, micro-restrainer information was kindly provided by Neville and colleagues.

The graphical abstract and Figure 1B were created with BioRender.com under license by RS and a group license provided by CRC/TR 296.

CONFLICTS OF INTEREST

The authors declare no competing financial interests.

APPENDIX A. SUPPLEMENTARY DATA

Supplementary data to this article can be found online at https://doi.org/10.1016/j.molmet.2022.101563.

REFERENCES

[1] Arruda, A.P., Pers, B.M., Parlakgul, G., Guney, E., Inouye, K., Hotamisligil, G.S., 2014. Chronic enrichment of hepatic endoplasmic reticulum-mitochondria contact leads to mitochondrial dysfunction in obesity. Nature Medicine 20(12):1427—1435.

[2] de Mello, A.H., Costa, A.B., Engel, J.D.G., Rezin, G.T., 2018. Mitochondrial dysfunction in obesity. Life Sciences 192:26—32.

[3] Bournat, J.C., Brown, C.W., 2010. Mitochondrial dysfunction in obesity. Current Opinion in Endocrinology Diabetes and Obesity 17(5):446—452.

[4] Xu, H., Barnes, G.T., Yang, Q., Tan, G., Yang, D., Chou, C.J., et al., 2003. Chronic inflammation in fat plays a crucial role in the development of obesity-related insulin resistance. Journal of Clinical Investigation 112(12):1821—1830.

[5] Pilling, D., Karhadkar, T.R., Gomer, R.H., 2021. High-fat diet-induced adipose tissue and liver inflammation and steatosis in mice are reduced by inhibiting sialidases. American Journal of Pathology 191(1):131—143.

[6] Weisberg, S.P., McCann, D., Desai, M., Rosenbaum, M., Leibel, R.L., Ferrante Jr., A.W., 2003. Obesity is associated with macrophage accumulation in adipose tissue. Journal of Clinical Investigation 112(12):1796–1808.

[7] Shoelson, S.E., Herrero, L., Naaz, A., 2007. Obesity, inflammation, and insulin resistance. Gastroenterology 132(6):2169–2180.

[8] Kusminski, C.M., Scherer, P.E., 2012. Mitochondrial dysfunction in white adipose tissue. Trends in Endocrinology and Metabolism 23(9):435–443.

[9] Abdullah, A., Peeters, A., de Courten, M., Stoelwinder, J., 2010. The magnitude of association between overweight and obesity and the risk of diabetes: a meta-analysis of prospective cohort studies. Diabetes Research and Clinical Practice 89(3):309–319.

[10] Wiseman, M., 2008. The second World Cancer Research Fund/American Institute for Cancer Research expert report. Food, nutrition, physical activity, and the prevention of cancer: a global perspective. Proceedings of the Nutrition Society 67(3):253–256.

[11] Knight, J.A., 2011. Diseases and disorders associated with excess body weight. Annals of Clinical Laboratory Science 41(2):107–121.

[12] Paradies, G., Paradies, V., Ruggiero, F.M., Petrosillo, G., 2014. Oxidative stress, cardiolipin and mitochondrial dysfunction in nonalcoholic fatty liver disease. World Journal of Gastroenterology 20(39):14205–14218.

[13] Mansouri, A., Gattolliat, C.H., Asselah, T., 2018. Mitochondrial dysfunction and signaling in chronic liver diseases. Gastroenterology 155(3):629–647.

[14] Peng, K.Y., Watt, M.J., Rensen, S., Greve, J.W., Huynh, K., Jayawardana, K.S., et al., 2018. Mitochondrial dysfunction-related lipid changes occur in nonalcoholic fatty liver disease progression. The Journal of Lipid Research 59(10): 1977–1986.

[15] Sunny, N.E., Bril, F., Cusi, K., 2017. Mitochondrial adaptation in nonalcoholic fatty liver disease: novel mechanisms and treatment strategies. Trends in Endocrinology and Metabolism 28(4):250–260.

[16] Boland, M.L., Oldham, S., Boland, B.B., Will, S., Lapointe, J.M., Guionaud, S., et al., 2018. Nonalcoholic steatohepatitis severity is defined by a failure in compensatory antioxidant capacity in the setting of mitochondrial dysfunction. World Journal of Gastroenterology 24(16):1748–1765.

[17] Koliaki, C., Szendroedi, J., Kaul, K., Jelenik, T., Nowotny, P., Jankowiak, F., et al., 2015. Adaptation of hepatic mitochondrial function in humans with nonalcoholic fatty liver is lost in steatohepatitis. Cell Metabolism 21(5):739–746.

[18] Yin, X., Lanza, I.R., Swain, J.M., Sarr, M.G., Nair, K.S., Jensen, M.D., 2014. Adipocyte mitochondrial function is reduced in human obesity independent of fat cell size. Journal of Clinical Endocrinology and Metabolism 99(2):E209–E216.

[19] Wessels, B., Honecker, J., Schottl, T., Stecher, L., Klingenspor, M., Hauner, H., et al., 2019. Adipose mitochondrial respiratory capacity in obesity is impaired independently of glycemic status of tissue donors. Obesity 27(5):756–766.

[20] Madamanchi, N.R., Runge, M.S., 2007. Mitochondrial dysfunction in atherosclerosis. Circulation Research 100(4):460–473.

[21] Mercer, J.R., Cheng, K.K., Figg, N., Gorenne, I., Mahmoudi, M., Griffin, J., et al., 2010. DNA damage links mitochondrial dysfunction to atherosclerosis and the metabolic syndrome. Circulation Research 107(8):1021–1031.

[22] Zorzano, A., Liesa, M., Palacin, M., 2009. Role of mitochondrial dynamics proteins in the pathophysiology of obesity and type 2 diabetes. The International Journal of Biochemistry & Cell Biology 41(10):1846–1854.

[23] King, A., Selak, M.A., Gottlieb, E., 2006. Succinate dehydrogenase and fumarate hydratase: linking mitochondrial dysfunction and cancer. Oncogene 25(34):4675–4682.

[24] Cassim, S., Raymond, V.A., Lapierre, P., Bilodeau, M., 2017. From in vivo to in vitro: major metabolic alterations take place in hepatocytes during and following isolation. PLoS One 12(12):e0190366.

[25] Kuznetsov, A.V., Veksler, V., Gellerich, F.N., Saks, V., Margreiter, R., Kunz, W.S., 2008. Analysis of mitochondrial function in situ in permeabilized muscle fibers, tissues and cells. Nature Protocols 3(6):965–976.

[26] Neville, K.E., Bosse, T.L., Klekos, M., Mills, J.F., Weicksel, S.E., Waters, J.S., et al., 2018. A novel ex vivo method for measuring whole brain metabolism in model systems. Journal of Neuroscience Methods 296:32–43.

[27] Kespohl, M., Bredow, C., Klingel, K., Voss, M., Paeschke, A., Zickler, M., et al., 2020. Protein modification with ISG15 blocks coxsackievirus pathology by antiviral and metabolic reprogramming. Science Advances 6(11): eaay1109.

[28] Brachs, S., Polack, J., Brachs, M., Jahn-Hofmann, K., Elvert, R., Pfenninger, A., et al., 2019. Genetic nicotinamide N-methyltransferase (NNMT) deficiency in male mice improves insulin sensitivity in diet-induced obesity but does not affect glucose tolerance. Diabetes 68(3):527–542.

[29] Brachs, S., Winkel, A.F., Tang, H., Birkenfeld, A.L., Brunner, B., Jahn-Hofmann, K., et al., 2016. Inhibition of citrate cotransporter Slc13a5/mINDY by RNAi improves hepatic insulin sensitivity and prevents diet-induced non-alcoholic fatty liver disease in mice. Molecular Metabolism 5(11):1072–1082.

[30] Schreyer, S., Berndt, N., Eckstein, J., Mulleder, M., Hemmati-Sadeghi, S., Klein, C., et al., 2021. Dietary-challenged mice with Alzheimer-like pathology show increased energy expenditure and reduced adipocyte hypertrophy and steatosis. Aging (Albany NY) 13(8):10891–10919.

[31] Readnower, R.D., Brainard, R.E., Hill, B.G., Jones, S.P., 2012. Standardized bioenergetic profiling of adult mouse cardiomyocytes. Physiological Genomics 44(24):1208–1213.

[32] Takeichi, Y., Miyazawa, T., Sakamoto, S., Hanada, Y., Wang, L., Gotoh, K., et al., 2021. Non-alcoholic fatty liver disease in mice with hepatocyte-specific deletion of mitochondrial fission factor. Diabetologia 64(9):2092–2107.

[33] Oeckl, J., Bast-Habersbrunner, A., Fromme, T., Klingenspor, M., Li, Y., 2020. Isolation, culture, and functional analysis of murine thermogenic adipocytes. STAR Protocol 1(3):100118.

[34] Marchetti, P., Fovez, Q., Germain, N., Khamari, R., Kluza, J., 2020. Mitochondrial spare respiratory capacity: mechanisms, regulation, and significance in non-transformed and cancer cells. The FASEB Journal 34(10):13106–13124.

[35] Harman, D., 1956. Aging: a theory based on free radical and radiation chemistry. Journal of Gerontology 11(3):298–300.

[36] Nakamura, S., Takamura, T., Matsuzawa-Nagata, N., Takayama, H., Misu, H., Noda, H., et al., 2009. Palmitate induces insulin resistance in H4IIEC3 hepatocytes through reactive oxygen species produced by mitochondria. Journal of Biological Chemistry 284(22):14809–14818.

[37] Florez-Duquet, M., Horwitz, B.A., McDonald, R.B., 1998. Cellular proliferation and UCP content in brown adipose tissue of cold-exposed aging Fischer 344 rats. American Journal of Physiology 274(1):R196–R203.

[38] Gohlke, S., Zagoriy, V., Cuadros Inostroza, A., Meret, M., Mancini, C., Japtok, L., et al., 2019. Identification of functional lipid metabolism biomarkers of brown adipose tissue aging. Molecular Metabolism 24:1–17.

[39] Halestrap, A.P., 1987. Glucagon treatment of rats activates the respiratory chain of liver mitochondria at more than one site. Biochimica et Biophysica Acta 927(2):280–290.

[40] Jensen, C.B., Sistare, F.D., Hamman, H.C., Haynes Jr., R.C., 1983. Stimulation of mitochondrial functions by glucagon treatment. Evidence that effects are not artifacts of mitochondrial isolation. Biochemical Journal 210(3):819–827.

[41] LaNoue, K.F., Strzelecki, T., Finch, F., 1984. The effect of glucagon on hepatic respiratory capacity. Journal of Biological Chemistry 259(7):4116–4121.

[42] Nisoli, E., Tonello, C., Cardile, A., Cozzi, V., Bracale, R., Tedesco, L., et al., 2005. Calorie restriction promotes mitochondrial biogenesis by inducing the expression of eNOS. Science 310(5746):314–317.

[43] Schweizer, S., Oeckl, J., Klingenspor, M., Fromme, T., 2018. Substrate fluxes in brown adipocytes upon adrenergic stimulation and uncoupling protein 1 ablation. Life Science Alliance 1(6):e201800136.

[44] Cummins, T.D., Holden, C.R., Sansbury, B.E., Gibb, A.A., Shah, J., Zafar, N., et al., 2014. Metabolic remodeling of white adipose tissue in obesity. American Journal of Physiology. Endocrinology and Metabolism 307(3):E262–E277.

[45] Maekawa, R., Seino, Y., Ogata, H., Murase, M., Iida, A., Hosokawa, K., et al., 2017. Chronic high-sucrose diet increases fibroblast growth factor 21 production and energy expenditure in mice. The Journal of Nutritional Biochemistry 49:71—79.

[46] Xu, J., Lloyd, D.J., Hale, C., Stanislaus, S., Chen, M., Sivits, G., et al., 2009. Fibroblast growth factor 21 reverses hepatic steatosis, increases energy expenditure, and improves insulin sensitivity in diet-induced obese mice. Diabetes 58(1):250—259.

[47] Coskun, T., Bina, H.A., Schneider, M.A., Dunbar, J.D., Hu, C.C., Chen, Y., et al., 2008. Fibroblast growth factor 21 corrects obesity in mice. Endocrinology 149(12):6018—6027.

[48] Adams, A.C., Yang, C., Coskun, T., Cheng, C.C., Gimeno, R.E., Luo, Y., et al., 2012. The breadth of FGF21's metabolic actions are governed by FGFR1 in adipose tissue. Molecular Metabolism 2(1):31—37.

[49] Stanford, K.I., Middelbeek, R.J., Townsend, K.L., An, D., Nygaard, E.B., Hitchcox, K.M., et al., 2013. Brown adipose tissue regulates glucose homeostasis and insulin sensitivity. Journal of Clinical Investigation 123(1):215—223.

[50] Darcy, J., McFadden, S., Fang, Y., Huber, J.A., Zhang, C., Sun, L.Y., et al., 2016. Brown adipose tissue function is enhanced in long-lived, male ames dwarf mice. Endocrinology 157(12):4744—4753.

[51] Li, Y., Knapp, J.R., Kopchick, J.J., 2003. Enlargement of interscapular brown adipose tissue in growth hormone antagonist transgenic and in growth hormone receptor gene-disrupted dwarf mice. Experimental Biology and Medicine 228(2):207—215.

[52] Ortega-Molina, A., Efeyan, A., Lopez-Guadamillas, E., Munoz-Martin, M., Gomez-Lopez, G., Canamero, M., et al., 2012. Pten positively regulates brown adipose function, energy expenditure, and longevity. Cell Metabolism 15(3):382—394.

[53] Vatner, D.E., Zhang, J., Oydanich, M., Guers, J., Katsyuba, E., Yan, L., et al., 2018. Enhanced longevity and metabolism by brown adipose tissue with disruption of the regulator of G protein signaling 14. Aging Cell 17(4):e12751.

[54] Hacker, T.A., McKiernan, S.H., Douglas, P.S., Wanagat, J., Aiken, J.M., 2006. Age-related changes in cardiac structure and function in Fischer 344 x Brown Norway hybrid rats. American Journal of Physiology-Heart and Circulatory Physiology 290(1):H304—H311.

[55] Boengler, K., Kosiol, M., Mayr, M., Schulz, R., Rohrbach, S., 2017. Mitochondria and ageing: role in heart, skeletal muscle and adipose tissue. J Cachexia Sarcopenia Muscle 8(3):349—369.

[56] Vitorica, J., Cano, J., Satrustegui, J., Machado, A., 1981. Comparison between developmental and senescent changes in enzyme activities linked to energy metabolism in rat heart. Mechanism of Ageing and Development 16(2):105—116.

[57] Lancaster, T.S., Jefferson, S.J., Hunter, J.C., Lopez, V., Van Eyk, J.E., Lakatta, E.G., et al., 2012. Quantitative proteomic analysis reveals novel mitochondrial targets of estrogen deficiency in the aged female rat heart. Physiological Genomics 44(20):957—969.

[58] Cheng, Z., Ito, S., Nishio, N., Thanasegaran, S., Fang, H., Isobe, K., 2013. Characteristics of cardiac aging in C57BL/6 mice. Experimental Gerontology 48(3):341—348.

[59] Drahota, Z., Milerova, M., Stieglerova, A., Skarka, L., Houstek, J., Ostadal, B., 2005. Development of cytochrome-c oxidase activity in rat heart: down-regulation in newborn rats. Cell Biochemistry and Biophysics 43(1):87—94.

[60] Paradies, G., Petrosillo, G., Pistolese, M., Ruggiero, F.M., 2000. The effect of reactive oxygen species generated from the mitochondrial electron transport chain on the cytochrome c oxidase activity and on the cardiolipin content in bovine heart submitochondrial particles. FEBS Letters 466(2—3):323—326.

[61] Bolli, G.B., Fanelli, C.G., 1999. Physiology of glucose counterregulation to hypoglycemia. Endocrinology and Metabolism Clinics of North America 28(3):467—493.

[62] Rizza, R.A., 2010. Pathogenesis of fasting and postprandial hyperglycemia in type 2 diabetes: implications for therapy. Diabetes 59(11):2697—2707.

[63] MacDonald, P.E., De Marinis, Y.Z., Ramracheya, R., Salehi, A., Ma, X., Johnson, P.R., et al., 2007. A K ATP channel-dependent pathway within alpha cells regulates glucagon release from both rodent and human islets of Langerhans. PLoS Biology 5(6):e143.

[64] Allister, E.M., Robson-Doucette, C.A., Prentice, K.J., Hardy, A.B., Sultan, S., Gaisano, H.Y., et al., 2013. UCP2 regulates the glucagon response to fasting and starvation. Diabetes 62(5):1623—1633.

[65] Breton, L., Clot, J.P., Baudry, M., 1983. Effects of glucagon on basal metabolic rate and oxidative phosphorylation of rat liver mitochondria. Hormone and Metabolic Research 15(9):429—432.

[66] Yamazaki, R.K., Mickey, D.L., Story, M., 1980. Rapid action of glucagon on hepatic mitochondrial calcium metabolism and respiratory rates. Biochimica et Biophysica Acta 592(1):1—12.

[67] Yamazaki, R.K., 1975. Glucagon stimulation of mitochondrial respiration. Journal of Biological Chemistry 250(19):7924—7930.

[68] Munhoz, A.C., Vilas-Boas, E.A., Panveloski-Costa, A.C., Leite, J.S.M., Lucena, C.F., Riva, P., et al., 2020. Intermittent fasting for twelve weeks leads to increases in fat mass and hyperinsulinemia in young female wistar rats. Nutrients 12(4).

